

Predicting beach rotation using multiple atmospheric indices

Mark Wiggins¹, Tim Scott¹, Gerd Masselink¹, R. Jak McCarroll¹ & Paul Russell¹

*1. Coastal Processes Research Group, Plymouth University, Drake Circus, Plymouth
PL4 8AA, United Kingdom.*

Corresponding author: Mark Wiggins. mark.wiggins@plymouth.ac.uk

Abstract

Shoreline change in the form of beach rotation can occur at event to decadal timescales, especially in semi-sheltered embayments with bi-directional wave climates, leading to enhanced coastal vulnerability under predictions of increased sea level rise. Previous studies have shown that phases of winter-averaged atmospheric indices in the North Atlantic correlate with variations in average winter wave height and dominant direction; however, predictions of a localised wave climate and beach rotation from individual climate indices has exhibited limited skill. Here we show that the combination of two major north Atlantic climate indices, the North Atlantic Oscillation (NAO) and West Europe Pressure Anomaly (WEPA), improves the prediction of a wave power directionality index (WDI), known to correlate with beach rotation along the length of a headland bound gravel embayment. Results using a combination of NAO and WEPA, improves predictions of WDI with an associated R^2 of 0.66, when compared to 0.23 and 0.31 for NAO and WEPA individually. Hindcast (WDI_{WW3}) and index predicted (WDI_{Pred}) values of the WDI were shown to validate against measured beach rotation from 2008 to 2018 and modelled inshore potential longshore energy fluxes from 1980 to 2018. A long-term historic time series of WDI_{Pred} (1906-present) was then hindcast using records of NAO and WEPA. Qualitative validation of long-term beach rotation in response to the WDI_{Pred} is achieved with proxy records of beach change in the form of oblique and aerial photography and topographic maps. Low frequency (~60

25 years) beach rotation is shown to follow phases of the detrended cumulative WDI_{Pred} values,
26 over the period of 1906 to 2018, linked to the multi-decadal fluctuations in detrended
27 cumulative values of NAO and WEPA. When examined in the context of millennial-scale
28 proxy NAO records, it is clear the recent centennial-scale analysis does not capture past
29 variability and duration. This work has shown that: (1) potential future season ahead forecasts
30 of atmospheric indices may skilfully predict beach rotation in many regions with bi-
31 directional wave climates; and (2) historical analysis highlights the potential past phases of
32 extreme coastal realignment. These new insights will lead to proactive and informed
33 management from local authorities and coastal engineers.

34 Keywords: Beach rotation, NAO, WEPA, climate indices, atmospheric variability, N
35 Atlantic.

36 **1. Introduction**

37 Predicting shoreline change and evolution is an ever growing issue for coastal managers,
38 engineers and communities, particularly in light of observed and forecasted sea level rise
39 (Nicholls et al., 2011). Whilst increases in storminess and significant wave height (Dodet et
40 al., 2010) have been shown to cause significant cross-shore erosion of exposed beaches
41 (Burvingt et al., 2016; Masselink et al., 2016; Scott et al., 2016), beach rotation due to
42 longshore sediment transport under changes in the incoming wave direction (Klein et al.,
43 2002), plays an equally important role in coastal vulnerability for many semi-sheltered
44 embayments with bi-directional wave climates (Ruiz de Alegria-Arzaburu and Masselink,
45 2010; Wiggins et al., 2019a). Single storm events and annual winter rotational responses can
46 leave embayments depleted of sediment at the up-wave extent, reducing overall beach
47 volume and increasing the risk of damage, flooding and cliff retreat. If the wave climate
48 maintains a bias towards a particular direction over multi-annual to decadal timescales, these

49 potential risks increase, due to the lack of recovered beach volumes, reducing the protection
50 offered against damage under storm wave attack.

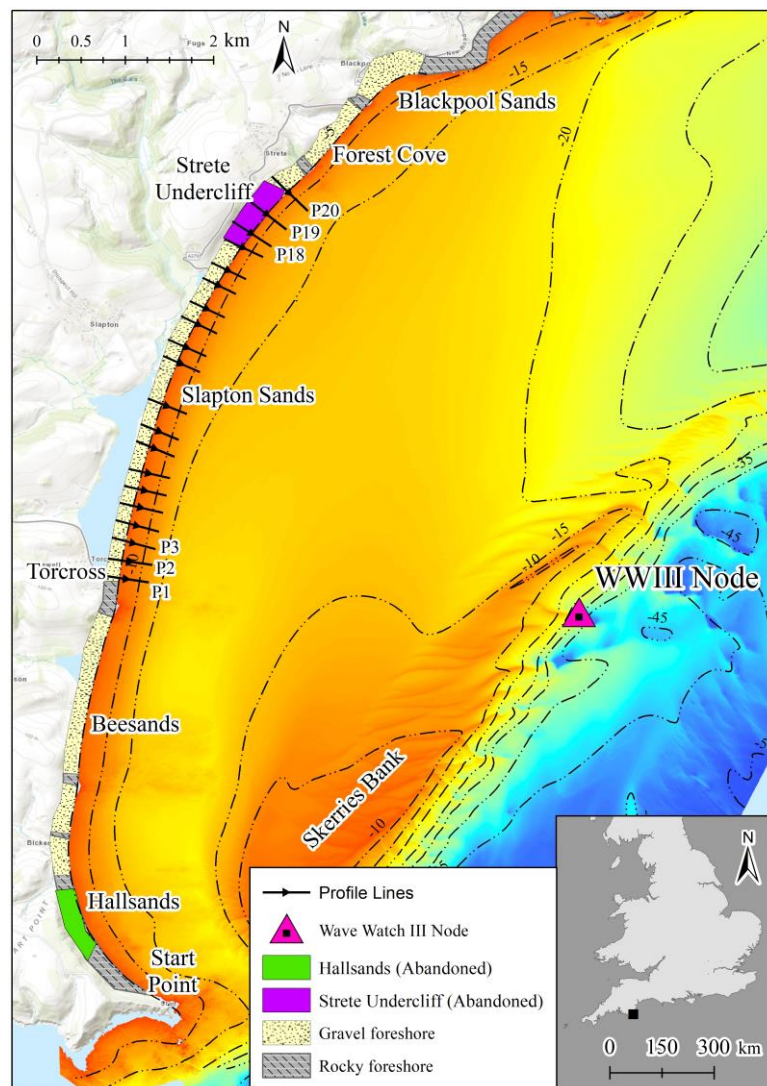
51 Understanding the controls that wave power and direction have on beach response has been
52 investigated globally, with phases of atmospheric indices showing strong links to wave height
53 and direction on local to basin wide scales (Barnard et al., 2015; Harley et al., 2017;
54 Ranasinghe et al., 2004). Within the North Atlantic, recent studies have identified both the
55 North Atlantic Oscillation (NAO) and West Europe Pressure Anomaly (WEPA) as playing a
56 significant role in controlling both the winter-averaged wave height and dominant wind
57 directions (Bacon and Carter, 1993; Castelle et al., 2018, 2017; Dodet et al., 2010; Izaguirre
58 et al., 2010; Martínez-Asensio et al., 2016; Plomaritis et al., 2015). Positive phases of the
59 NAO have been shown to predict increased winter wave height and westerly winds in the
60 upper latitudes of the north Atlantic, northward of 52° N, whilst positive phases of WEPA
61 outscore other indices in predicting increased wave heights southward of this latitude, until
62 the coast of Portugal (Castelle et al., 2018). Along the entire length of the south coast of the
63 United Kingdom (<52° N), where waves are directionally bi-modal (south-westerly and
64 easterly), Wiggins et al. (2019b) observed that winter NAO and WEPA were best suited to
65 predicting easterly and south-westerly winter-averaged wave power, respectively, with weak
66 or no correlation in their opposite directions. In turn, the beach response for many south-east
67 facing beaches along the same coastline, showed rotation was controlled by the Wave
68 Directional Index (WDI), defined as the standardised winter power balance between the
69 primary and secondary winter wave directions (Wiggins et al., 2019a). Despite the strong
70 correlations between WDI and beach rotation, individually, NAO and WEPA were only
71 weakly positively correlated with the WDI, and only significantly correlated with beach
72 rotation in two of the 22 measured locations.

73 Given the current state of winter NAO forecasting (Dunstone et al., 2016; Scaife et al., 2015;
74 Weisheimer et al., 2017), and the ability to predict several months ahead for the coming
75 winter season, any improvements to our understanding of the relationship between
76 atmospheric indices and morphology could lead us towards season ahead beach response
77 forecasts for rotational sites, a tool that would be welcomed by coastal managers from local
78 to regional scales. Furthermore, an improved relationship between climate variability and
79 beach response could offer the capability to investigate historic beach state, providing a
80 representative indicator of potential future variability, and place the observed contemporary
81 changes into a longer-term context. For example, centurial-scale reconstructions of the NAO
82 (Cook et al., 2002; Faust et al., 2016; Trouet et al., 2012) and the use of proxy records to
83 model the NAO as far back as 3000BP (e.g. Baker et al., 2015), suggest that low frequency
84 fluctuations of significant magnitude have occurred over multi-centurial timescales, many of
85 which have been linked to well documented climate anomalies (e.g. Mediaeval Climate
86 Anomaly, Little Ice Age), causing variations in precipitation, temperature and storminess,
87 potentially driving large scale morphological activity such as sustained coastal dune
88 transgression (Clarke and Rendell, 2006; Jackson et al., 2019). This study aims to investigate
89 whether an improved relationship between climatic indices and winter WDI can be obtained
90 by multivariate analysis, helping to place our current observations of wave climate controls
91 on beach rotation into context with centurial scale fluctuations, allowing for proactive
92 decisions in terms of long-term planning and coastal management.

93 **2. Regional setting**

94 Start Bay lies along the south coast of Devon, United Kingdom (50.27° N, 3.65° W), facing
95 south east into the English Channel. The embayment consists of four interconnected coarse
96 gravel barriers ($D_{50} = 2 - 10\text{mm}$), backed by freshwater lagoons and separated at high tides by
97 protruding rocky headlands and wave cut platforms. Aligned from south-west to north-east,

98 its wave climate is bi-directional, consisting of predominantly diminished Atlantic swell
 99 waves from the south-west and short fetch easterly wind waves from the English Channel.
 100 Offshore wave angles are modulated by the presence of Skerries Bank (McCarroll et al.,
 101 2020) and Start Point (Figure 1), which refract and attenuate south-westerly waves to become
 102 southerly at the shoreline, whilst easterly waves maintain their angle as they propagate into
 103 the bay.



104
 105 Figure 1. Location map of Start Bay with bathymetric contours (UKHO, 2013) and W/III (Met Office) model
 106 node location. Topographic profile survey line locations are displayed as black arrows. The locations of two
 107 abandoned villages are displayed by the coloured polygons located towards the northern and southern ends of
 108 the embayment.

109 The southerly and easterly wave angles drive northward and southward sediment transport
110 respectively, and the embayment is continually in a state of dynamic equilibrium, with the
111 planform shape rotating in response to the current wave approach. The full embayment
112 sediment cell as a whole, was demonstrated to be closed by Wiggins et al. (2019a), bounded
113 by significant northern and southern headlands; however, beach rotation and exchange of
114 sediment between the individual sub-embayments was observed through headland bypassing
115 under extreme wave conditions (McCarroll et al., 2019) and sustained periods of a particular
116 wave direction (Wiggins et al., 2019a).

117 Both full-embayment and sub-embayment beach rotation has long been a concern within
118 Start Bay, with significant historical and contemporary examples being the subject of
119 numerous scientific studies (Chadwick et al., 2005; Hails, 1975; McCarroll et al., 2019;
120 Robinson, 1961; Ruiz de Alegria-Arzaburu and Masselink, 2010; Wiggins et al., 2019a,
121 2019b, 2017). The loss of the old village of Hallsands in 1917 is one of the highest profile
122 cases of coastal erosion impacts in the United Kingdom. Lying at the southern corner of Start
123 Bay (Figure 1), its collapse into the sea during a severe easterly storm followed a sustained
124 lowering of the beach level in the years earlier, largely attributed to the dredging of subtidal
125 beach material between 1897 and 1902 (Worth (1904), cited in May and Hansom (2003)). In
126 addition to the dredging, evidence suggests that beach lowering at this end of the embayment
127 was exacerbated due to a coincidental shift in winter NAO to a sustained positive phase for
128 almost 30 years from the commencement of dredging (1898), leading to increased southerly
129 waves, and clockwise rotation of the beach under prolonged northward sediment transport
130 (Wiggins et al., 2017). Historical accounts of an earlier lost village at the opposite end of
131 Start Bay, suggests the local community may have formed settlements based on the rotation
132 and planform of the beach. Strete Undercliff, a small fishing village formed during the early
133 17th century (Goodall, 2007) and located at the northern end of Slapton Sands (Figure 1), was

134 documented on early nautical maps (Denbigh, 2017), until its subsequent disappearance by
135 1780 (Stranack, 2017; Waterhouse, 2009), around the time the village of Hallsands (in the
136 south) became more established. Despite the lack of quantitative data from this period, it
137 could be suggested that due to the closed nature of the sediment budget within Start Bay
138 (Wiggins et al., 2019a), variations in multi-decadal phases of wave direction may have
139 influenced the settlement locations of the past and present communities of Start Bay.

140 More recently, during the winter of 2013/14, Start Bay's beaches experienced significant
141 clockwise rotation under a single winter season characterized by unprecedented south-
142 westerly storm events (Masselink et al., 2015; Scott et al., 2016; Wiggins et al., 2019a),
143 leaving the southern ends of embayments depleted of sediment. This increased the
144 vulnerability of coastal defences at southern beach extremities, and in the following winter
145 years (2015 and 2016), lack of beach volume resulted in the undermining and collapse of sea
146 walls at Torcross, Slapton Sands, and loss of infrastructure including the car park at
147 Hallsands (BBC, 2016).

148 **3. Materials and methods**

149

150 *3.1. Wave data*

151 WaveWatchIII modelled wave data was obtained for a coastal node offshore of Start Bay
152 (Figure 1) in approximately 20m water depth. Total winter wave power was computed at
153 each year for the period of December through March (DJFM), and subsequently split into
154 contributions of the primary (south westerly) and secondary (easterly) directions, designated
155 P_1 and P_2 , respectively.

156 The wave directionality index (WDI) was computed for each winter from 1980 to 2018 using
157 equation (1) as set out in (Wiggins et al., 2019a);

158
$$\text{WDI} = ((P_1 - P_2) - \overline{(P_1 - P_2)}) / \sigma(P_1 - P_2) \quad (1)$$

159 where $(P_1 - P_2)$ is the difference in wave power between the primary and secondary wave
160 directions, $\overline{(P_1 - P_2)}$ is the long-term mean and $\sigma(P_1 - P_2)$ is the long-term standard
161 deviation of that difference. Positive (negative) values of the WDI represent winter periods
162 where the wave climate was more southerly (easterly) than average.

163 *3.2. Atmospheric indices*

164 Winter averaged (DJFM) atmospheric index values for the station-based NAO (based on the
165 difference of normalized sea level pressure (SLP) between Lisbon, Portugal and
166 Stykkisholmur/Reykjavik, Iceland since 1864) were obtained from The Climate Data Guide
167 (downloaded from the National Center for Atmospheric Research,
168 <https://climatedataguide.ucar.edu/>). Additionally, values of the West Europe Pressure
169 Anomaly (WEPA) were obtained via hindcasts of SLP between s Valentia (Ireland) and
170 Santa Cruz de Tenerife (Canary Islands), as developed by Castelle et al (2017) from
171 Twentieth Century Reanalysis data (<https://www.esrl.noaa.gov/psd/>). Despite SLP derived
172 NAO records being available as far back as the mid to late 1800s, and proxy reconstructions
173 (described later in section 5) going even further up to 3000 years before present, records of
174 WEPA only date back to 1906 due to limited SLP records and inconsistent hindcasts beyond
175 this.

176 Previous studies along the entire length of the south coast of England (Wiggins et al., 2019b)
177 have shown that individual wave power contributions from the primary and secondary wave
178 directional modes are well correlated with WEPA and NAO respectively. Winter values of
179 the WDI for Start Bay are positively correlated with both NAO and WEPA, suggesting that a
180 combination of the two indices may improve the predictive skill at this location. To assess

181 this further, an empirical stepwise multiple linear regression (SMLR) model was constructed
182 using both NAO and WEPA.

183 3.3. Modelled longshore sediment flux

184 A look-up table modelling approach was applied by McCarroll et al. (2020), for the period
185 1980 – 2018, to transform offshore wave conditions to breakpoint values in order to estimate
186 alongshore wave power and potential longshore sediment flux within the Start Bay
187 embayment. The estimated flux is ‘potential’ as the model assumes unlimited sediment
188 availability. Bathymetry for the model was obtained using inshore multibeam (Wiggins et al.,
189 2019a), combined with offshore multibeam from 2013 (UKHO, 2013). To generate the
190 inshore wave conditions for the look-up model, Delft3D-WAVE was run in stationary mode
191 for ~400 scenarios, covering the full range of naturally occurring boundary wave conditions.
192 Boundary conditions for a 1980-2018 wave time series were obtained from a coarse-grid
193 hindcast model (WaveWatchIII, Met Office). These boundary conditions were transferred to
194 points along the 14-m depth contour using the look-up table approach. A simple refraction-
195 shoaling parameterisation (Van Rijn, 2014) was used to transform waves from 14-m depth to
196 the break point, with nodes at 25-m spacing. The breaking wave conditions were used to
197 estimate alongshore wave power using linear wave theory. Alongshore sediment flux was
198 estimated using the CERC equation (USACE, 2002), for a range of K-value coefficients (0.04
199 to 0.26). The output from the look-up model is a 38-year time series of longshore wave power
200 and potential sediment flux, which was validated against prior model results and field
201 observations (McCarroll et al., 2019). A detailed description of the model setup and forcing
202 can be found within McCarroll et al. (2020). Total winter transport was summed for the
203 DJFM months, and at each location, correlations were drawn between both the observed WDI
204 and the predicted WDI.

229 al. (2019a) as being indicative of beach rotation, with a significant negative correlation with
230 the northern end of Slapton Sands, implying beach width at one end of the embayment can be
231 used as an indicator of beach rotation. In total, 32 oblique photographs were used, taken from
232 the same location (dating from 1875 to 2019), without the need for rectification. In addition,
233 seven sets of aerial photography (1944 to 2017), and three geo-rectified OS maps with high
234 and low water contours (1887, 1852 and 1983) were also used.

235 To assess historical changes in beach width with the limited dataset available, an integer scale
236 of -2 (“Very Narrow”) to +2 (“Very Wide”) was assessed qualitatively (as shown in Figure
237 7), based on manual interpretation of the entire dataset, providing a simple, categorical metric
238 of relative beach width for each dated photograph and map for this location. The range of
239 observed beach widths was taken into account in devising the scale, from the most accreted in
240 1890, to most eroded in 2016.

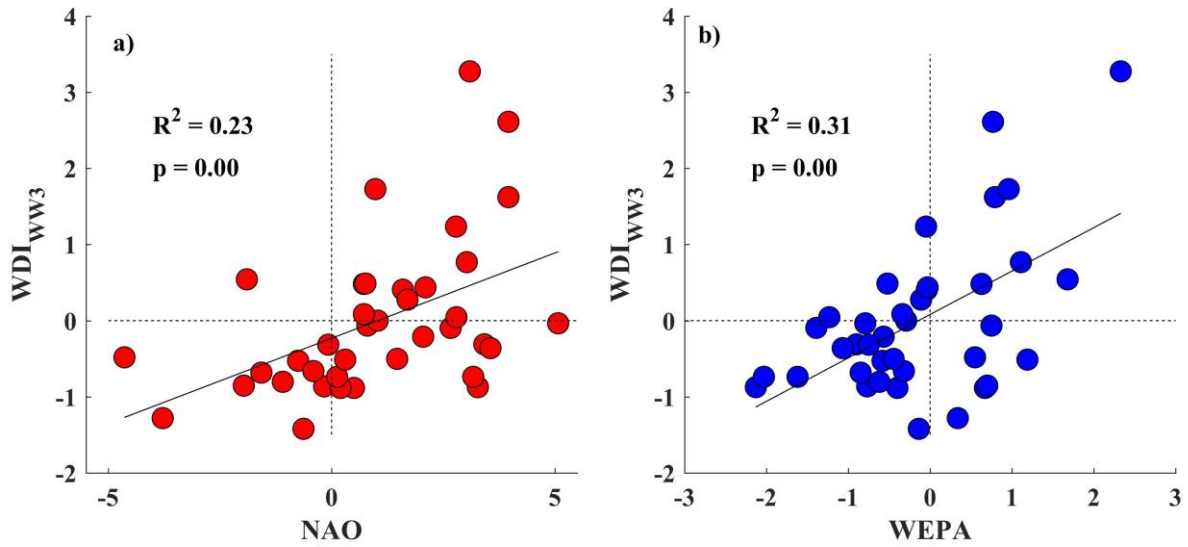
241 **4. Results**

242

243 *4.1. WDI predictions from atmospheric indices*

244 Initial exploration of the relationships between the WaveWatchIII derived WDI (WDI_{WW3})
245 with NAO and WEPA, for a 38 year timeseries between 1980 and 2018 show statistically
246 significant ($p < 0.05$) positive correlations (Figure 2); however, relative skill in predicting the
247 WDI_{WW3} is low for both indices ($R^2 < 0.31$).

248



249

250 Figure 2. Correlations between winter averaged atmospheric indices NAO, WEPA and the WDI_{WW3} for the
 251 period of 1980 to 2018.

252 A SMLR model was created using both NAO and WEPA as predictor variables, with results
 253 suggesting that a regression model computed from a combination both NAO and WEPA
 254 variables provide improvement in the skill of predicted WDI (WDI_{Pred}). First and second
 255 order polynomial models were tested, in addition to two-term exponential regressions, with a
 256 linear fit offering the most explanatory power in predicting the WDI_{Pred} , such that;

$$257 \quad WDI_{Pred} = \beta_0 + \beta_1 NAO + \beta_2 WEPA \quad (3)$$

258 Where β_0 represents the intercept and β_1 to β_2 are coefficients of the predictor variables, with
 259 their estimates, confidence bounds and statistics shown in Table 1.

260 Table 1: SMLR model statistics for the predictor variables used for modelling winter values of the WDI.

<i>Coefficient</i>	<i>Predictor</i>	<i>Estimate</i>	<i>Lower (95%)</i>	<i>Upper (95%)</i>	<i>SE</i>	<i>tStat</i>	<i>pValue</i>
β_0	(Intercept)	-0.19	-0.41	0.03	0.11	-1.78	0.083
β_1	NAO	0.29	0.19	0.38	0.05	6.11	5.54×10^{-7}
β_2	WEPA	0.69	0.48	0.90	0.10	6.74	8.36×10^{-8}

261

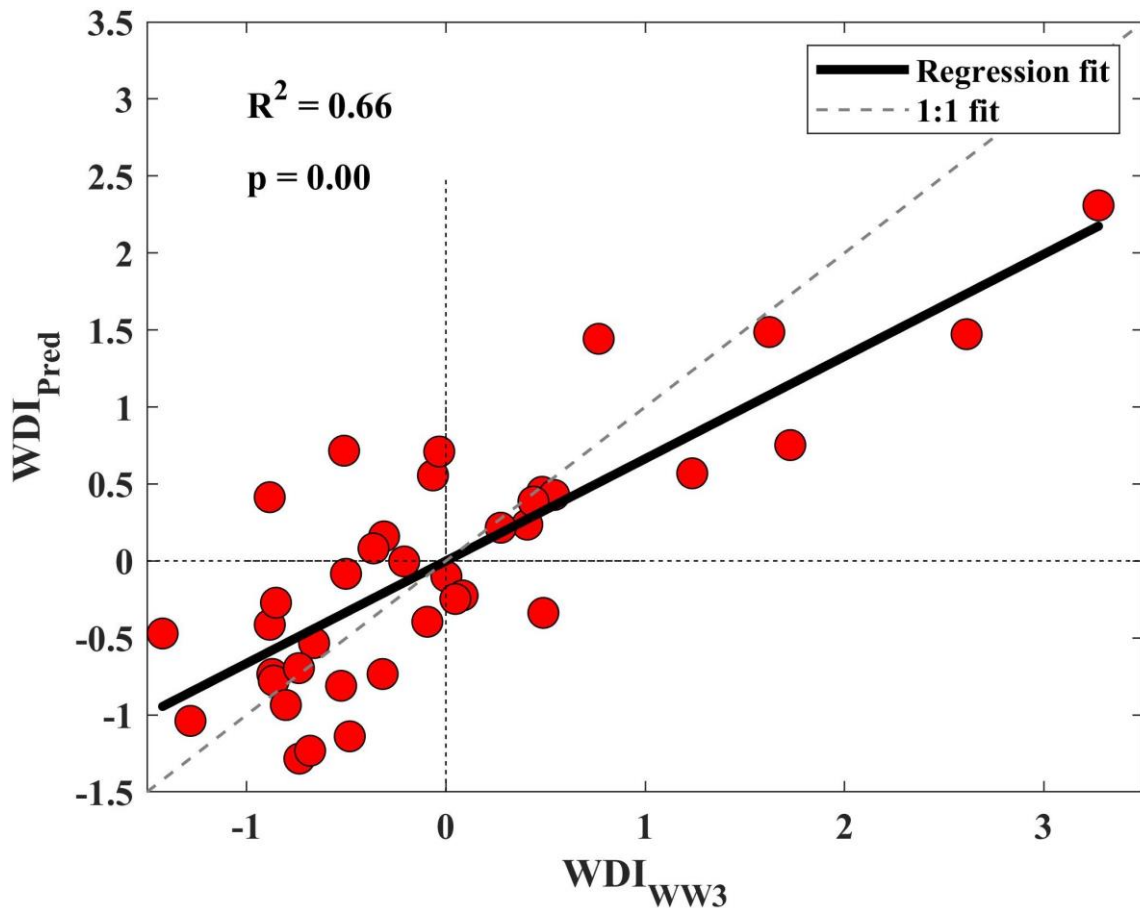
262 Overall improvements to the predictive skill of combining the indices are shown in Table 2,
 263 with the RMSE reducing from 0.9 when using NAO alone, to 0.60 when using NAO and
 264 WEPA. Similar improvements are seen when assessing the R^2 value, with an improvement of
 265 from 0.23 to 0.66 ($p = 4.71 \times 10^{-10}$). The coefficients for the two indices (Table 1) show that
 266 WEPA contributes more (0.69) to the overall predicted values of the WDI_{Pred} than NAO
 267 (0.29).

268 Table 2: Improvements to the SMLR models statistics for a range of input variables and sum index used for
 269 predicting winter values of the WDI_{Pred} .

<i>Predictor Terms</i>	<i>RMSE</i>	<i>R-squared</i>	<i>P-value</i>
NAO	0.90	0.23	2.39×10^{-3}
WEPA	0.86	0.31	3.15×10^{-4}
NAO + WEPA	0.60	0.66	5.08×10^{-9}

270

271 Outputs of WDI_{Pred} for the period of the modelled wave data (Figure 4) show the addition of
 272 both indices reproduce the winter WDI_{WW3} values with an R^2 value of 0.66.



273

274 Figure 3. WDI_{WW3} for the winter periods of 1980 to 2018 plotted against WDI_{Pred} predicted using a SMLR
 275 model of winter atmospheric indices. The regression fit is shown as the bold line, whilst the 1:1 fit is displayed
 276 as the dashed grey line.

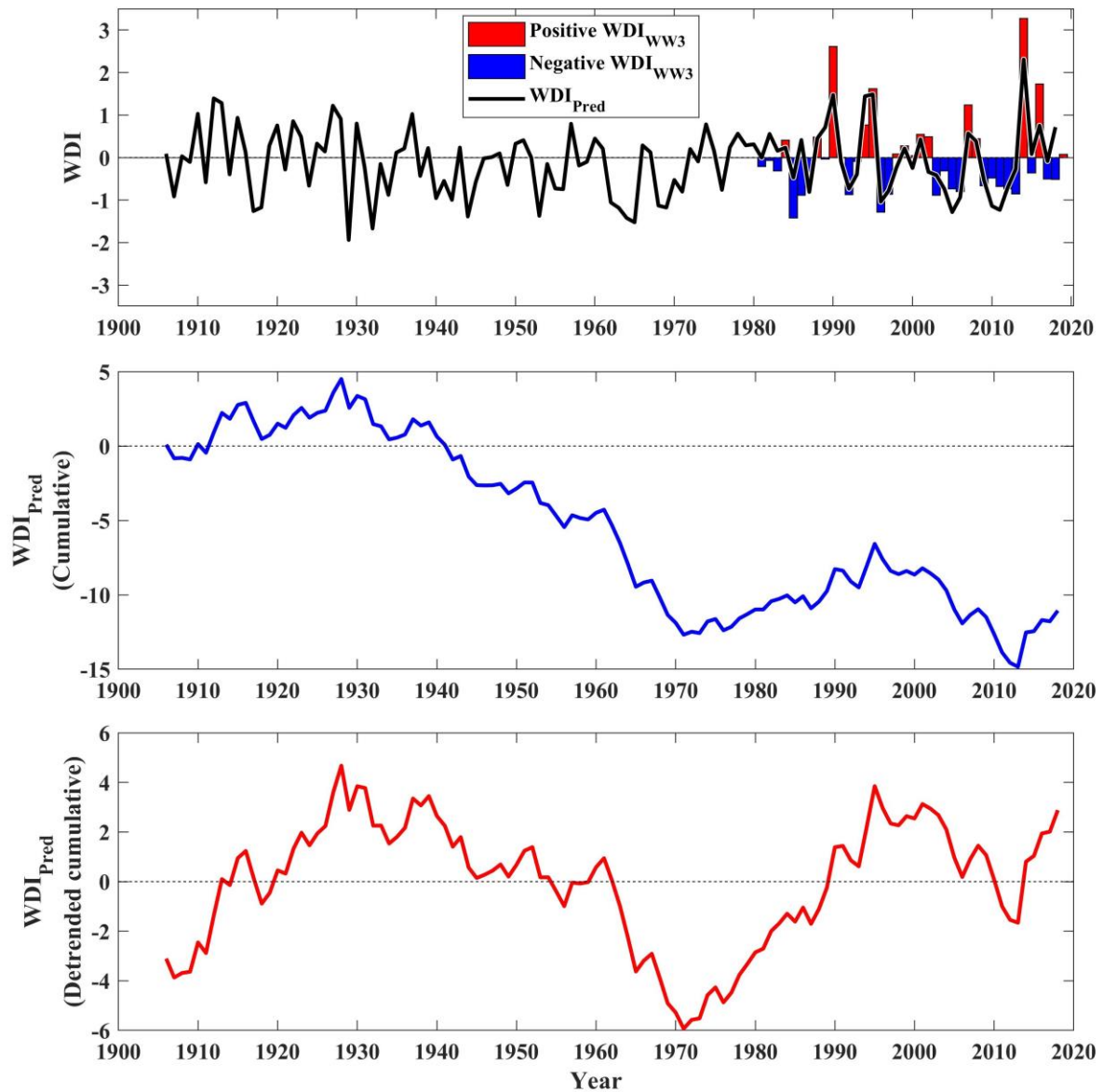
277 Using the regression model, values of NAO and WEPA are used to hindcast the WDI_{Pred} back
 278 to the beginning of the record of atmospheric indices (1906). The predicted output can be
 279 seen in the top panel of Figure 4, with the accumulated value of the WDI_{Pred} plotted in the
 280 middle panel.

281 Clear inter-annual variation can be seen within the long-term WDI_{Pred} values (Figure 4 a);
 282 however, there are periods of sustained negative or positive winter values, persisting for up to
 283 five years in a row (e.g. 2008 to 2013). Despite the high R² value between the WDI_{WW3} and
 284 the WDI_{Pred} hindcast from atmospheric indices (for the overlapping period of 1980 to 2018,
 285 Figure 3), there are some years where the sign of the WDI_{Pred} is opposite to the WDI_{WW3}, e.g.

286 2000 to 2003. This can be attributed to years where winter averaged values of NAO and
287 WEPA are low (close to zero) or opposite in sign, leading to the larger of the two indices
288 impacting the WDI_{Pred} . In addition, although the regression analysis was conducted using a
289 linear relationship, the fit between winter averaged climate indices and WDI_{WW3} is not
290 perfectly linear, especially for extremely high values of NAO and WEPA within the limited
291 37-year timeseries (Figure 2a and b). This explains why the regression model under predicts
292 the value of the WDI_{Pred} for some years; however, in the majority of cases where the WDI_{WW3}
293 is either highly positive or negative, hindcast values of the WDI_{Pred} share the same sign and
294 are also larger in magnitude relative to the overall time series average.

295 The annual hindcast WDI_{Pred} values have a limited trend over the last 113 years; however, the
296 cumulative WDI_{Pred} values (Figure 4b) show a negative trend of -0.165 yr^{-1} . Hindcast
297 cumulative WDI_{Pred} was detrended by removing the linear mean trend using a least-squares
298 regression, to highlight the fluctuations in the cumulative WDI_{Pred} values over time. The
299 detrended values of the cumulative WDI_{Pred} (Figure 4c, bottom panel) indicate that there is
300 potential periodicity in phases of positive and negative WDI_{Pred} .

301



302

303 Figure 4. a) SMLR modelled WDI_{Pred} values from atmospheric indices NAO and WEPA, predicted back to
 304 1906, as well as the values of WDI_{WW3} as obtained from the WaveWatchIII model. b) The cumulative WDI_{Pred}
 305 values from 1906 to 2018, as predicted by the SMLR model of NAO and WEPA. c) The detrended cumulative
 306 values of WDI_{Pred} from 1906 to 2018.

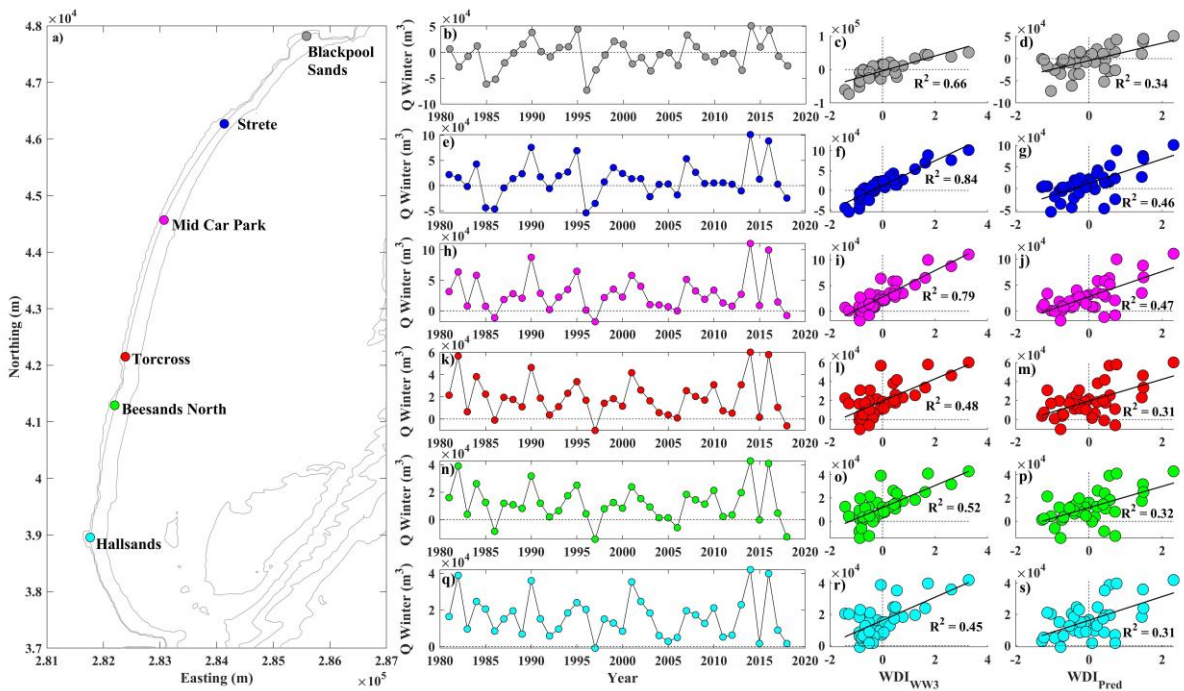
307 *4.2. Modelled longshore sediment flux*

308 To examine the relationship between the two different offshore WDI parameters (WDI_{WW3}
 309 and WDI_{Pred}) and transport rates within the embayment, potential along-shore sediment flux
 310 was computed for a series of six fixed shoreline positions (Figure 5.a), using an inshore wave

311 transformation model comprising real bathymetry (see further, McCarroll et al. (2020)). Total
 312 potential winter transport totals (Figure 5.b, e, h, k, n, q) were compared with WDI_{WW3} values
 313 for the period of 1980 to 2018. In all locations, significant positive correlations are observed
 314 between the WDI_{WW3} and directional sediment transport (Figure 5.c, f, i, l, o, r), with the
 315 strongest correlation being at Strete ($R^2 = 0.84$), the northern end of Slapton Sands (Figure
 316 5.f). Other nodes located in the northern sections of the embayment show a balance of
 317 northward (southward) transport under highly positive (negative) WDI_{WW3} winters, whereas
 318 almost all winter WDI_{WW3} conditions drive northward transport at Hallsands in the far south
 319 of the embayment.

320 The positive correlations throughout the bay suggest that the WDI_{WW3} calculated at the
 321 offshore model node is an adequate proxy of the balance of inshore wave directions,
 322 responsible for driving sediment transport and beach rotation within the embayment.

323



324

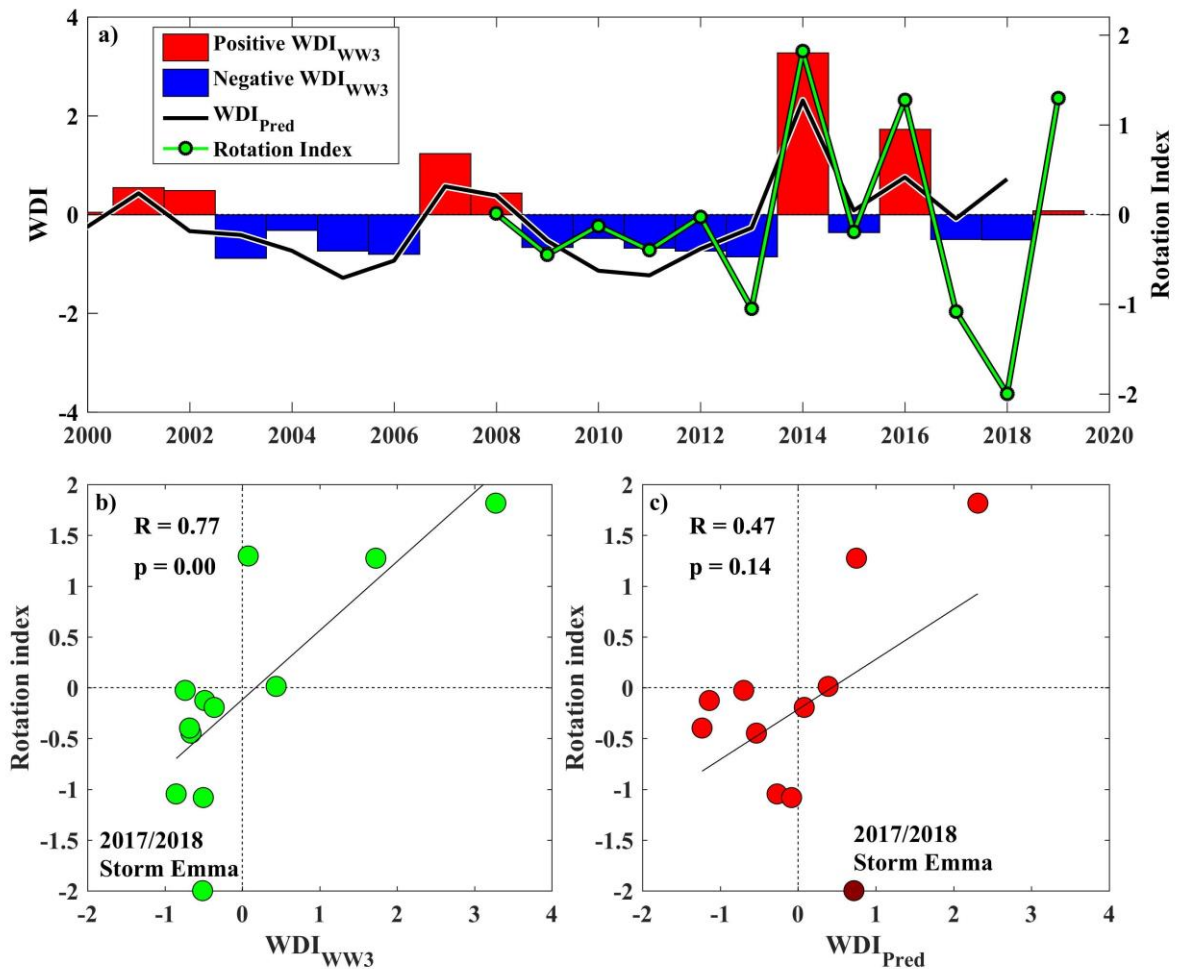
325 Figure 5. a) location map of inshore nodes at which total potential winter sediment flux has been calculated, b)
326 total potential winter alongshore sediment flux at Blackpool Sands, e) Strete, h) Middle car park, k) Torcross, n)
327 Beesands North and q) Hallsands. Panels c), f), i), l), o) and r) show the correlation between the WDI_{WW3} , and
328 longshore sediment transport at the six locations, whilst panels d), g), j), m), p) and s) show the same
329 correlations but with values of WDI_{Pred} .

330 In addition to the comparisons between modelled sediment transport and WDI_{WW3} , the same
331 comparison was conducted against values of the WDI_{Pred} , as produced by the SMLR (Figure
332 5 d, g, j, m, p and s). At all sites, weaker but similarly positive correlations were observed,
333 with all results being significant at the 95% confidence interval, highlighting that the WDI_{Pred}
334 computed from climate indexes is a suitable proxy for estimating flux at the shoreline.
335 Although the WDI_{Pred} values are consistently lower than the WDI_{WW3} (in part due to the
336 standardized nature of the WDI wave power parameter)

337 4.3. Validation against beach surveys and historical records

338 To demonstrate the potential application of WDI_{Pred} in predicting beach rotation, correlations
339 with contemporary and historical beach rotation are presented. Similar to previous studies of
340 both Slapton Sands and other locations in the south west, values of the WDI_{WW3} are well
341 correlated with the rotation index (defined in eq. 2) for the period of 2008 to 2019, derived
342 from topographic survey data. The sign of the rotation index tracks well with the sign of
343 WDI_{WW3} (Figure 6.a), whilst the linear correlation of the two is significant and strong ($R =$
344 0.77 , $p = 0.00$, Figure 6.b). Similarly, the correlation between the WDI_{Pred} and rotation index
345 is positive ($R = 0.47$), despite not being statistically significant at the 95% confidence limit;
346 however, it is observed that the correlation is much stronger and statistically significant ($R =$
347 0.74 , $p = 0.01$), if the winter change from 2017/18 (due to a single easterly event) is removed
348 as an outlier (discussed further in Section 5).

349



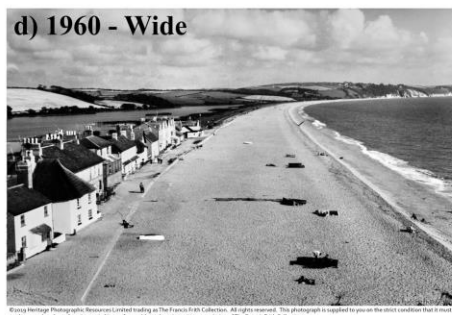
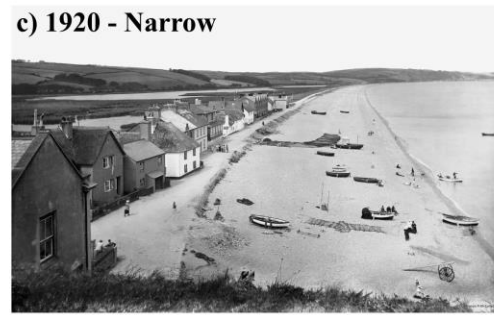
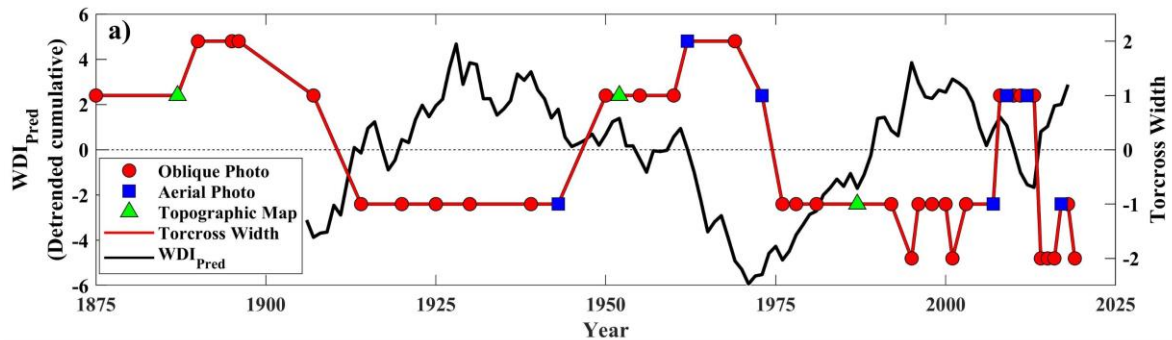
350

351 Figure 6. a) Time series of short term (~20 years) WDI_{WW3} values, shown by the red and blue bars, overlaid with
 352 WDI_{Pred} from the NAO and WEPA SMLR model, shown as the black line. The rotation index (green line) over
 353 the period of 2008 to 2019, derived from measured winter change (November to March) in beach volume at
 354 opposing ends of Slapton Sands, with positive (negative) values indicating northward clockwise (southward
 355 anticlockwise) beach rotation. b) Correlation between WDI_{WW3} and winter rotation index for the period of 2008
 356 to 2019. c) Correlation between winter WDI_{Pred} and the winter rotation index for the period of 2008 to 2018.

357 The lack of consistent high-quality shoreline data before 2006 means proxy records are the
 358 only possibility for validation of the longer-term WDI_{Pred} values. Time series of the
 359 qualitative beach width assessment for Torcross and the detrended cumulative WDI_{Pred} values
 360 for the period spanning 1906 to 2019 are shown in Figure 7.a. The beach appears widest
 361 during the last decade of the 1800s, then beginning to narrow up to the 1920's, remaining a
 362 similar width in photographs and maps until around 1945. A period of beach widening then

363 occurs until the early 1970's, before narrowing again until 2016, the lowest beach volume in
 364 both the short-term surveys, and photo archive.

365

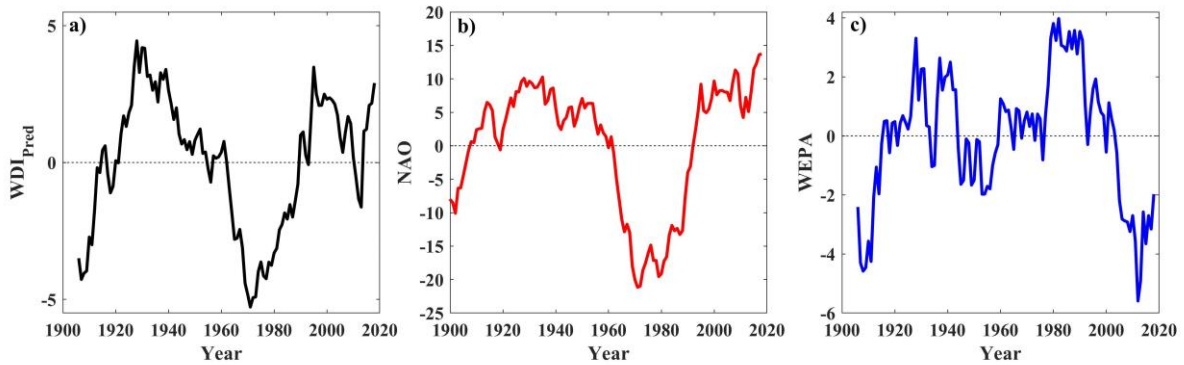


366

367 Figure 7. a) Detrended cumulative values of the WDI_{Pred} (left axis) from 1906 to 2018, overlaid on the right axis
 368 is a qualitative assessment of beach width at Torcross (southern end of Slapton Sands), with positive values
 369 indicating a wide beach, suggesting southward sediment transport and anticlockwise beach rotation, whilst
 370 negative values indicate a narrower beach, signifying a period of potential northward sediment transport and
 371 clockwise beach rotation. b) Photos of Torcross taken in 1890, c) 1920, d) 1960 (Copyright The Francis Frith
 372 Collection) e) 2016 (Copyright G. Masselink), showing different beach widths throughout the last 200 years.

373 Both beach width and detrended cumulative WDI_{Pred} values display low frequency
 374 fluctuations over the last 113 years, with beach width appearing to narrow during periods of

375 cumulative positive WDI_{Pred} and widen during sustained negative phases (Figure 7.a). Long-
376 term detrended cumulative values for the WDI_{Pred} as well as the NAO and WEPA were
377 computed and the results are displayed in Figure 8.



378

379 Figure 8. Detrended cumulative values of winter averaged a) WDI_{Pred} , b) NAO and c) WEPA.

380 For the WDI_{Pred} values (Figure 8.a), the data appears to show a multi-decadal variation in
381 cumulative positive and negative phases, whilst the NAO (Figure 8.b) and WEPA (Figure
382 8.c) display similar scale variations (Figure 8.c).

383 5. Discussion

384 This study has shown that combining two major winter-averaged climate indices, NAO and
385 WEPA, in a SMLR model significantly improves skill when trying to predict winter-averaged
386 offshore directional wave climate (WDI), when compared to using the individual indices.
387 Given that the WDI is key predictor of the magnitude and direction of beach rotation at this,
388 and many similar sites along the length of the southern UK coastline (Wiggins et al., 2019b),
389 the ability to forecast its value from two significant indices represents a step forward in
390 assessing the accuracy in historical records of beach rotation, and the future potential to
391 predict wave climate and morphological behaviour at seasonal to centurial timescales. Whilst
392 previous studies have been able to link changes in atmospheric variability to deviations in
393 wave height or direction (Barnard et al., 2015; Burvingt et al., 2018; Castelle et al., 2018,

394 2017; Dodet et al., 2010; Harley et al., 2017; Ranasinghe et al., 2004), the combination of
395 multiple indices for direct calculation of a bi-directional wave climate parameter for opposing
396 directions is unique.

397 Both the WDI_{WW3} and WDI_{Pred} were shown to correlate with winter integrated potential
398 longshore transport rates throughout the embayment (McCarroll et al., 2020). Statistically
399 significant ($p < 0.05$) correlation coefficients for WDI_{WW3} and WDI_{Pred} ranging from 0.67 to
400 0.92, and 0.56 to 0.68, respectively, show that the WDI calculated for a single point offshore
401 is a robust proxy for the inshore wave climate and sediment transport. Similar to this study,
402 significant correlations were found by Splinter et al. (2012) between yearly modelled net
403 longshore transport rates and positive phases of the Inter-decadal Pacific Oscillation (IPO)
404 and the Southern Oscillation Index (SOI); however, regression models combining both
405 indices required a five-year smoothing average of both predictor and response variables, in
406 addition to separate model equations for positive and negative phases of the IPO,
407 incorporating different coefficients and predictor values at different time lags. The simplicity
408 of the SMLR model used in this study, suggests that where WDI calculations are well
409 correlated with beach rotation (Wiggins et al., 2019a, 2019b), similar analysis can be
410 conducted at other rotation dominated sites.

411 The results of Section 4.3 show the rotation index of Slapton Sands (as calculated from >10
412 year topographic survey record) is well correlated with values of the WDI_{WW3} , but not
413 significantly correlated with the atmospheric index based WDI_{Pred} values predicted by the
414 model over a 10-year period of observations. Further investigation into the limited dataset
415 showed that the winter of 2017/18 featured a large single easterly storm event (Storm Emma,
416 further description in (McCarroll et al., 2019)) which caused a significant counter clockwise
417 rotation of the beach at the end of the winter season (March 2nd 2018). The morphological
418 response was observed in the anti-clockwise rotational beach record and the observed

419 negative WDI_{ww3} value (-0.51); however, it was not reflected in the positive winter
420 averages of NAO and WEPA (0.30 and 1.17 respectively). As a result, such values of
421 atmospheric indices resulted in the model predicting a positive WDI_{Pred} value ($+0.70$),
422 suggesting a more southerly than average dominance of wave power. That winter also stands
423 out as having the highest anti-clockwise rotation index during the observational period, so its
424 impact on reducing the strength of the correlation coefficient is substantial.

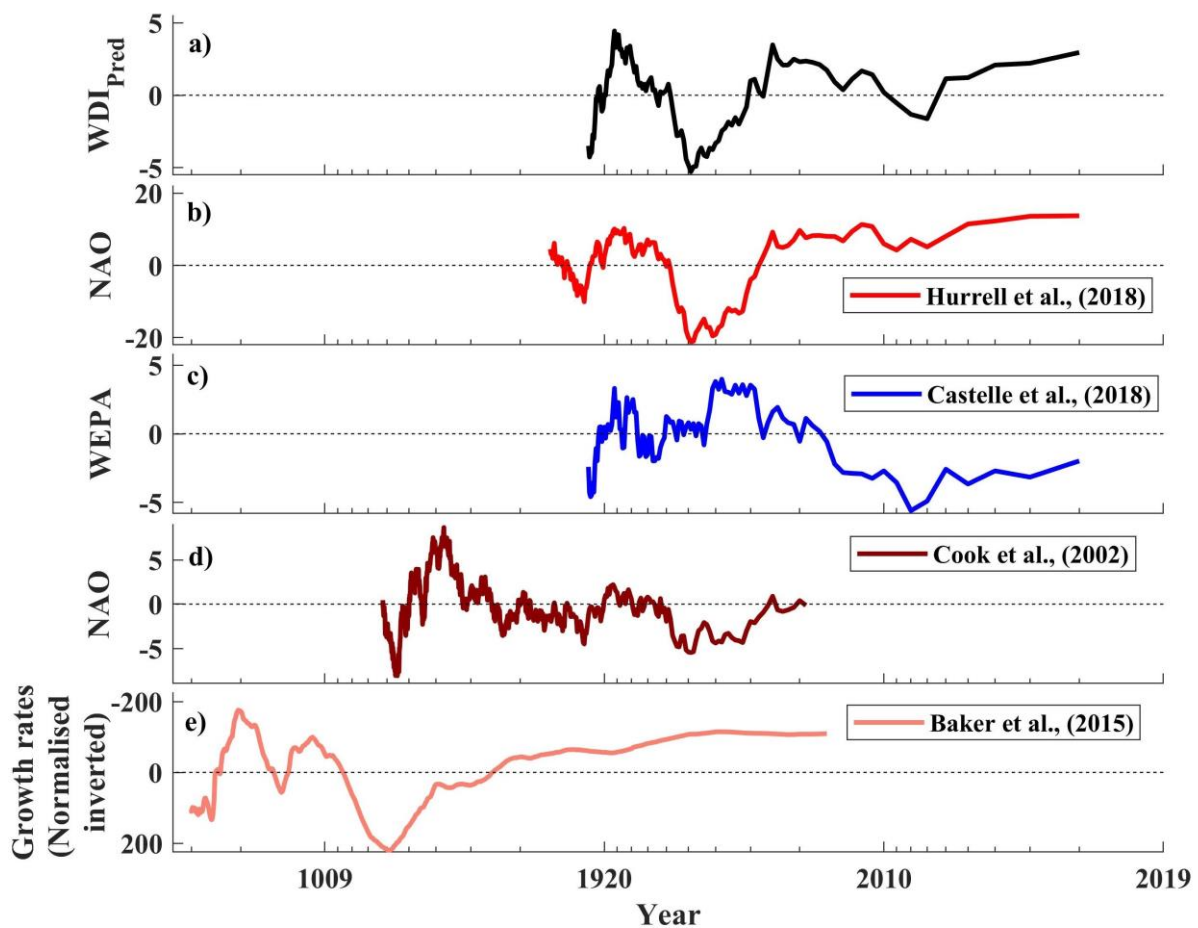
425 Clearly single extreme events such as this can cause significant beach rotation and substantial
426 damage to infrastructure, and whilst the WDI_{Pred} is shown to correlate well with beach
427 rotation when the 2017/18 winter is removed from the analysis ($R = 0.74$ $p = 0.01$), ignoring
428 potential outliers of the general trend presents problems in application within a coastal
429 management setting. If a longer period of accurate morphological survey data was available,
430 better understanding of the skill and limitations of the relationship between WDI_{Pred} and
431 beach rotation could be obtained.

432 Beyond the immediate correlations between both winter WDI values and recent multi-annual
433 beach rotation, it is interesting to examine the detrended cumulative record of WDI_{Pred} as
434 conceptually it provides insights into the rotational state of the embayment. Using the SMLR
435 model a hindcast record of WDI_{Pred} shows low frequency (~ 60 - 70 years) multi-decadal
436 fluctuations over the last century (Figure 8), driven by combined changes in the cumulative
437 values of winter NAO and WEPA. Although the methodology for constructing a proxy record
438 of observed beach rotation is quantitatively limited (i.e. manual interpretation of southern
439 beach width from photography and topographic maps), it does present a qualitative coherence
440 with the periodicity in the long-term cumulative WDI_{Pred} values (Figure 7a). Temporal gaps
441 and lack of consistency in the seasonal timing of photographs may lead to aliasing of higher
442 frequency variations in beach width, but the longer-term signal presented in the historical
443 record shows a clear coherence with the detrended cumulative WDI_{Pred} values, providing

444 some validation for using detrended cumulative WDI_{Pred} in this context. Several decades of
445 the last century which show a positive phases in detrended cumulative WDI_{Pred} values (e.g.
446 1900 to 1930; sustained southerly winter waves) coincide with periods of beach narrowing
447 (clockwise rotation), whilst phases of sustained negative detrended cumulative WDI_{Pred}
448 values (e.g. 1940 to 1970; higher percentage of easterly winter waves) coincide with beach
449 widening (anti-clockwise rotation). Current improvements to shoreline detection from
450 satellite images dating back to the 1980s, could provide the extended datasets required (e.g.
451 Vos et al., 2019), and would further assist in validating regression models of atmospheric
452 indices and their control on wave climates and beach response.

453 Successive winters of the same WDI_{Pred} sign (positive or negative) may drive cumulative
454 beach rotation in a particular direction or maintain the planform shape if already rotated.
455 Event-scale wave action can cause rapid changes to the beach profile and planform shape,
456 and reversals of wave direction have been shown to quickly counter-rotate the embayment's
457 of Start Bay (McCarroll et al., 2019; Ruiz de Alegria-Arzaburu and Masselink, 2010;
458 Wiggins et al., 2019a); however, this study has identified that multi-decadal trends in the
459 detrended cumulative WDI_{Pred} , are mirrored in beach rotation proxies over the last 113 years.
460 Such multi-decadal beach rotation patterns have been identified in other locations over a
461 comparable time period, such as the south coast of Pembrokeshire, Wales, UK, with similar
462 correlations found between wave angle variations driving beach rotation under contrasting
463 phases of the NAO (Thomas et al., 2013). The longer-term trends in cumulative WDI values
464 appear to dictate the general planform state of Start Bay, indicating that within the next 100
465 years, a continued upward trend in cumulative WDI values, or a potential phase shift into a
466 sustained negative period may lead to sustained clockwise rotation or reversal and anti-
467 clockwise rotation.

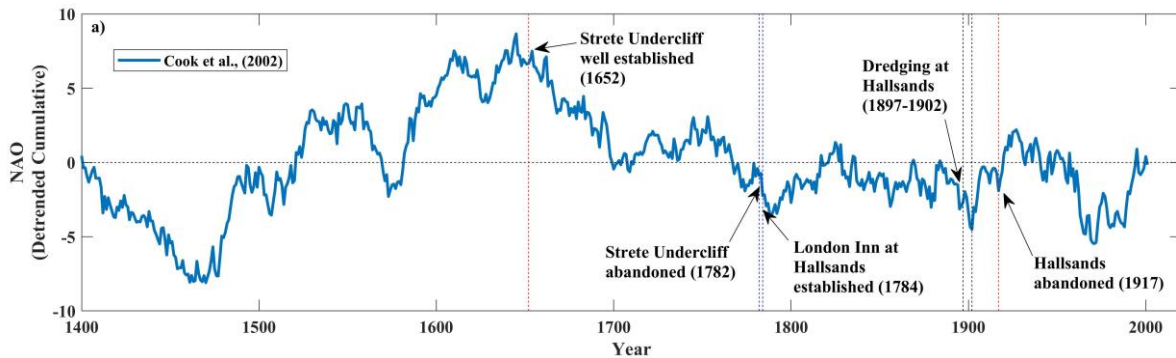
468 To place the observed contemporary changes in context with long-term reconstructions of the
 469 NAO, detrended cumulative values of the WDI_{Pred} , NAO and WEPA from the current study
 470 are plotted on a log time scale in Figure 9. a, b, and c. For comparison, detrended cumulative
 471 values of two extended NAO reconstructions are also presented. The first (Figure 9. d), dating
 472 back to 1400, is derived from tree-ring and ice-core proxies from Cook et al. (2002)The
 473 second (Figure 9. e) is presented as a ~3000 year record of detrended cumulative normalised
 474 stalagmite growth rates (Baker et al., 2015), inverted for ease of comparison, with high
 475 growth rates representative of drier conditions, reflective of negative NAO phases.



476
 477 Figure 9. Detrended cumulative values of a) WDI_{Pred} , b) NAO from Hurrell et al., (2018) c) WEPA derived by
 478 Castelle et al., (2018), d) long-term NAO reconstructions from Cook et al., (2002), e) normalised stalagmite
 479 growth rates (inverted) from Baker et al., (2015). Time in year date (A.D.) is presented on a log scale.

480 Both additional records demonstrate sustained multi-decadal to multi-centurial phases of
481 significant magnitude which have been confirmed by several other authors (e.g. Faust et al.,
482 2016; Trouet et al., 2012). These observed fluctuations are of significantly greater scale and
483 duration than those exhibited within the 113 years assessed in this study. Long-term
484 variations in NAO have seen noticeable climate shifts identified in Europe over the last 2000
485 years, including a relative warming during the MCA (~800 to 1300 A.D.) due to persistent
486 positive NAO (Trouet et al., 2009), as well as a cooler period during the LIA (~1400 – 1850
487 A.D.) linked to a persistent negative NAO phase (Luterbacher et al., 2002). European coastal
488 response to these changes has been documented, with large-scale dune growth and inland
489 sand migration evidenced during the LIA under negative NAO conditions, due to increased
490 sand availability and stronger onshore winds (Clarke and Rendell, 2006), as well as cooler
491 temperatures limiting vegetation growth and destabilising dunes (Jackson et al., 2019).
492 Historical accounts of many settlements and agricultural land being abandoned due to wind
493 driven sand migration throughout Europe (Clarke and Rendell, 2009), indicates that
494 atmospheric effects on coastal communities have been always been apparent, driving a
495 constant need for shoreline adaptation. Within the context of the present study site, the
496 shoreline of Start Bay has likely undergone many previous sustained rotational states,
497 evidenced by the loss of two historical settlements at opposing ends of the embayment
498 (Figure 1), Strete Undercliff and Hallsands (Wiggins et al., 2017), within only the last 300
499 years. Exact dates of Strete Undercliff's formation are unclear, but it was well established by
500 1652 A.D. at the northern end of the embayment, likely following a sustained positive phase
501 of cumulative NAO winters (Figure 10), driving clockwise rotation and northward sediment
502 transport, resulting in a wide beach. It's eventual decline and demise 130 years later (1782
503 A.D.) followed an opposing phase of cumulative negative NAO winters, possibly driving
504 anti-clockwise rotation and southward sediment transport. Around the same time, early

505 records of the formation of Hallsands, in the southern corner of the embayment, suggest
 506 anticlockwise rotation produced a wider beach and encouraged settlement at this location,
 507 before dredging of beach shingle (Worth, 1904) and a reversal towards more positive NAO
 508 winters at the turn of the 20th century (Wiggins et al., 2017), depleted the protective beach
 509 and the village was abandoned in 1917.



510

511 Figure 10. Detrended cumulative NAO reconstruction from Cook et al. (2002), with annotations describing the
 512 establishment and subsequent demise of two historic settlements within Start Bay, Strete Undercliff in the north,
 513 and Hallsands in the south.

514 The observed low frequency variations in long-term NAO suggests that sustained
 515 morphological rotations may have been occurring over substantially longer timescales in
 516 Start Bay, and much of Europe, particularly in rotation prone sites where wave climates are
 517 bi-directional.

518 The skill demonstrated in using combined NAO and WEPA for predicting the WDI and
 519 hence beach rotation, leads to the question of whether skilful forecasts of both indices can be
 520 obtained for either short-term (seasonal) or longer-term (multi-annual to decadal) timescales.
 521 Given that Castelle et al. (2017) have shown that NAO and WEPA are not correlated,
 522 independent forecasts of each index would need to be made well ahead of the coming winter
 523 season if the predictability of the WDI can be achieved at timescales useful to coastal
 524 managers. For example, Colman et al. (2011) made use of the NAO's positive correlation

525 with wave height in the North Sea, to predict expected operational downtime of oil and gas
526 rigs using season ahead forecasts of the NAO, made available several months in advance;
527 however, our work presents the ability, and therefore enhanced application, of predicting the
528 direction and magnitude of the wave power balance in a region where it significantly impacts
529 coastal rotation and subsequent vulnerability. Improvements to seasonal NAO forecasts are
530 currently being showcased by many authors (Baker et al., 2018; Dunstone et al., 2016; Scaife
531 et al., 2015; Wang et al., 2017); however, hindcast predictions of the NAO over the last 100
532 years has shown that forecast skill may be variable, with particular weakness during sustained
533 phases of low magnitude negative NAO winters, and better skill during the stronger, positive
534 phases during the beginning and end of the 20th century (Weisheimer et al., 2017). The results
535 of the present study and several previous research efforts (Wiggins et al., 2019a, 2019b)
536 highlight that the NAO's strong negative correlation with easterly wave events is critical in
537 the formulation of WDI values for the present location. In this case study, skilful prediction
538 of negative NAO winters is crucial for identifying the anti-clockwise rotations observed
539 during increased easterly waves. WEPA has been shown to have much greater skill in
540 predicting the occurrence of the more dominant south-westerly waves but, as yet, is largely
541 unpredictable at the season-ahead timescale, in part due to current climate models reliance on
542 accurate predictions of winter mean SLP, which are weaker for the areas around the UK and
543 Ireland (Scott et al., in prep.), leading to a lack of forecast skill in areas where NAO has little
544 influence, and WEPA is unresolved.

545 **6. Conclusions**

546 This study has shown that a combination of two major atmospheric indices significantly
547 improves the predictive skill for a SMLR model of the bi-directional winter wave power
548 balance (WDI), which in turn has been shown to directly control morphological beach
549 rotation on shorter to multi-annual timescales. The model was then used to hindcast WDI_{Pred}

550 using long-term records of NAO and WEPA, with the detrended cumulative values showing
551 periodicity linked to similar fluctuations in detrended cumulative values of both indices.
552 Further results showed that trends in the WDI_{Pred} are mirrored in the historic records of beach
553 rotation for this site, suggesting that beyond seasonal and event-scale rotational events, the
554 long-term planform of this, and many similar embayments may be controlled by multi-
555 decadal to centurial scale trends in phases of atmospheric indices.

556 Application of this multi-index regression method suggests that the increased ability to
557 predict climate indices some months in advance of the coming winter period, may allow for
558 season-ahead forecasts of forthcoming wave climates, and hence potential rotational beach
559 impacts. Practically, this would provide coastal managers with an informed forecast of likely
560 risks in high-impact areas, enabling proactive decisions to be made regarding hard or soft
561 engineering works within rotational sites.

562 The following conclusions of this study are as follows;

- 563 1. Increased skilful prediction ($R^2 = 0.66$) of the WDI_{Pred} was be obtained from a
564 regression model comprised of two atmospheric indices, when compared to the skill
565 of individual indices alone.
566
- 567 2. Modelled alongshore wave power and potential sediment flux at fixed shoreline
568 positions were significantly correlated with observed and predicted WDI at a range of
569 locations within the study site; suggesting that the WDI is a valid proxy for inshore
570 sediment transport.
571
- 572 3. Medium term (10-year) measured beach rotation correlates with the observed and
573 model predicted WDI record (with the exception of an individual extreme event),

574 showing multiple atmospheric indices may hindcast beach rotational state at many
575 other locations, given extensive and reliable records.

576

577 4. Longer-term records of low frequency NAO phases suggest that larger scale rotational
578 events may have occurred at multi-centurial timescales, driving shoreline adaptation
579 of communities in response to variations in climate indices.

580

581 **Acknowledgements**

582 This research was funded by the U.K. Natural Environment Research Council,
583 Grant Number NE/M004996/1; BLUE-coast project.

584 The authors would like to thank the United Kingdom Meteorological Office, The Climate
585 Data Guide, Bruno Castelle, Guillaume Dodet and Plymouth Coastal Observatory.

586

587 **Data availability**

588 WaveWatchIII datasets are available from the Climate index data for NAO is available at

589 <https://climatedataguide.ucar.edu/climate-data/hurrell-north-atlantic-oscillation-nao-index->

590 [station-based](https://climatedataguide.ucar.edu/climate-data/hurrell-north-atlantic-oscillation-nao-index-station-based) .Climate index data for WEPA index is available at

591 https://www.esrl.noaa.gov/psd/data/gridded/data.20thC_ReanV2.html . Topographic survey

592 data from Plymouth University's monthly monitoring programme is archived at the British

593 Oceanographic Data Centre (BODC), available at <https://www.bodc.ac.uk/data/> . Topographic

594 maps are available at <https://digimap.edina.ac.uk/os> . Historical oblique photographs are

595 available at <https://www.francisfrith.com> whilst aerial photographs can be obtained from

596 <http://southwest.coastalmonitoring.org/> .

597

598 **References**

- 599 British Broadcasting Corporation, BBC, 2016. High tide causes Torcross sea wall collapse
600 and Devon road closure. Available at: [https://www.bbc.co.uk/news/uk-england-devon-](https://www.bbc.co.uk/news/uk-england-devon-35558922)
601 [35558922](https://www.bbc.co.uk/news/uk-england-devon-35558922) (Accessed: 17 October 2019).
- 602 Bacon, S., Carter, D.J.T., 1993. A connection between mean wave height and atmospheric
603 pressure gradient in the North Atlantic. *Int. J. Climatol.* 13, 423–436.
604 <https://doi.org/10.1002/joc.3370130406>
- 605 Baker, A., C. Hellstrom, J., Kelly, B.F.J., Mariethoz, G., Trouet, V., 2015. A composite
606 annual-resolution stalagmite record of North Atlantic climate over the last three
607 millennia. *Sci. Rep.* 5, 10307.
- 608 Baker, L.H., Shaffrey, L.C., Sutton, R.T., Weisheimer, A., Scaife, A.A., 2018. An
609 Intercomparison of Skill and Overconfidence/ Underconfidence of the Wintertime North
610 Atlantic Oscillation in Multimodel Seasonal Forecasts. *Geophys. Res. Lett.* 45, 7808–
611 7817. <https://doi.org/10.1029/2018GL078838>
- 612 Barnard, P.L., Short, A.D., Harley, M.D., Splinter, K.D., Vitousek, S., Turner, I.L., Allan, J.,
613 Banno, M., Bryan, K.R., Doria, A., Hansen, J.E., Kato, S., Kuriyama, Y., Randall-
614 Goodwin, E., Ruggiero, P., Walker, I.J., Heathfield, D.K., 2015. Coastal vulnerability
615 across the Pacific dominated by El Niño/Southern Oscillation. *Nat. Geosci.* 8, 801.
- 616 Burvingt, O., Masselink, G., Russell, P., Scott, T., 2016. Beach response to consecutive
617 extreme storms using LiDAR along the SW coast of England. *J. Coast. Res.* 75, 1052–
618 1056. <https://doi.org/10.2112/si75-211.1>
- 619 Burvingt, O., Masselink, G., Scott, T., Davidson, M., Russell, P., 2018. Climate forcing of
620 regionally-coherent extreme storm impact and recovery on embayed beaches. *Mar.*

621 Geol. 401, 112–128. <https://doi.org/10.1016/j.margeo.2018.04.004>

622 Castelle, B., Dodet, G., Masselink, G., Scott, T., 2018. Increased Winter-Mean Wave Height,
623 Variability, and Periodicity in the Northeast Atlantic Over 1949–2017. *Geophys. Res.*
624 *Lett.* 45, 3586–3596. <https://doi.org/10.1002/2017GL076884>

625 Castelle, B., Dodet, G., Scott, T., 2017. A new climate index controlling winter wave activity
626 along the Atlantic coast of Europe : the West Europe Pressure Anomaly. *Geophys. Res.*
627 *Lett.* 44, 1384–1392. <https://doi.org/10.1002/2016GL072379>

628 Chadwick, A.J., Karunarathna, H., Gehrels, W.R., Massey, A.C., O’Brien, D., Dales, D.,
629 2005. A new analysis of the Slapton barrier beach system, UK. *Proc. Inst. Civ. Eng. -*
630 *Marit. Eng.* 158, 147–161. <https://doi.org/10.1680/maen.2005.158.4.147>

631 Clarke, M.L., Rendell, H.M., 2009. The impact of North Atlantic storminess on western
632 European coasts: A review. *Quat. Int.* 195, 31–41.
633 <https://doi.org/10.1016/j.quaint.2008.02.007>

634 Clarke, M.L., Rendell, H.M., 2006. Effects of storminess, sand supply and the North Atlantic
635 Oscillation on sand invasion and coastal dune accretion in western Portugal. *The*
636 *Holocene* 16, 341–355. <https://doi.org/10.1191/0959683606hl932rp>

637 Colman, A.W., Palin, E.J., Sanderson, M.G., Harrison, R.T., 2011. The Potential for Seasonal
638 Forecasting of Winter Wave Heights in the Northern North Sea. *Weather Forecast.* 26
639 (6), 1067–1074. <https://doi.org/10.1175/WAF-D-11-00017.1>

640 Cook, E.R., D’Arrigo, R.D., Mann, M.E., 2002. A Well-Verified , Multiproxy Reconstruction
641 of the Winter North Atlantic Oscillation. *J. Clim.* 15, 1754–1764.

642 Denbigh, A., 2017. The Slapton Line - Living with a Changing Coast. *F. Stud.* 1–4.

643 Dodet, G., Bertin, X., Taborda, R., 2010. Wave climate variability in the North-East Atlantic

644 Ocean over the last six decades. *Ocean Model.* 31, 120–131.
645 <https://doi.org/10.1016/J.OCEMOD.2009.10.010>

646 Dunstone, N., Smith, D., Scaife, A.A., Hermanson, L., Eade, R., Robinson, N., Andrews, M.,
647 Knight, J., 2016. Skilful predictions of the winter North Atlantic Oscillation one year
648 ahead. *Nat. Geosci.* 9, 809. <https://doi.org/https://doi.org/10.1038/ngeo2824>

649 Faust, J., Fabian, K., Milzer, G., Giraudeau, J., Knies, J., 2016. Norwegian fjord sediments
650 reveal NAO related winter temperature and precipitation changes of the past 2800 years.
651 *Earth Planet. Sci. Lett.* 435, 84–93. <https://doi.org/10.1016/j.epsl.2015.12.003>

652 Goodall, F., 2007. *Lost Devon*. Birliin Publishing.

653 Hails, J.R., 1975. *Offshore Morphology and Sediment Distribution, Start Bay, Devon*. *Philos.*
654 *Trans. R. Soc. London. Ser. A, Math. Phys. Sci.* 279, 221–228.

655 Harley, M.D., Turner, I.L., Kinsela, M.A., Middleton, J.H., Mumford, P.J., Splinter, K.D.,
656 Phillips, M.S., Simmons, J.A., Hanslow, D.J., Short, A.D., 2017. Extreme coastal
657 erosion enhanced by anomalous extratropical storm wave direction. *Sci. Rep.* 7, 6033.
658 <https://doi.org/10.1038/s41598-017-05792-1>

659 Hurrell, James, National Center for Atmospheric Research Staff, 2018. *The Climate Data*
660 *Guide: Hurrell North Atlantic Oscillation (NAO) Index (Station-based)*. Retrieved from.
661 [https://climatedataguide.ucar.edu/climate-data/hurrell-north-atlantic-oscillation-nao-](https://climatedataguide.ucar.edu/climate-data/hurrell-north-atlantic-oscillation-nao-index-station-based)
662 [index-station-based](https://climatedataguide.ucar.edu/climate-data/hurrell-north-atlantic-oscillation-nao-index-station-based).

663 Izaguirre, C., Mendez, F.J., Menendez, M., Luceño, A., Losada, I.J., 2010. Extreme wave
664 climate variability in southern Europe using satellite data. *J. Geophys. Res. Ocean.* 115.
665 <https://doi.org/10.1029/2009JC005802>

666 Jackson, D.W.T., Costas, S., Guisado-Pintado, E., 2019. Large-scale transgressive coastal

667 dune behaviour in Europe during the Little Ice Age. *Glob. Planet. Change* 175, 82–91.
668 <https://doi.org/10.1016/j.gloplacha.2019.02.003>

669 Klein, A.H.D.F., Filho, L.B., Schumacher, D.H., 2002. Short-Term Beach Rotation Processes
670 in Distinct Headland Bay Beach Systems. *J. Coast. Res.* 18, 442–458.
671 <https://doi.org/10.2307/4299093>

672 Luterbacher, J., Xoplaki, E., Dietrich, D., Jones, P.D., Davies, T.D., Portis, D., Storch, H.
673 Von, Gyalistras, D., Casty, C., Wanner, H., 2002. Extending North Atlantic Oscillation
674 reconstructions back to 1500. <https://doi.org/10.1006/asle.2001.0044>

675 Martínez-Asensio, A., Tsimplis, M.N., Marcos, M., Feng, X., Gomis, D., Jordà, G., Josey,
676 S.A., 2016. Response of the North Atlantic wave climate to atmospheric modes of
677 variability. *Int. J. Climatol.* 36, 1210–1225. <https://doi.org/10.1002/joc.4415>

678 Masselink, G., Castelle, B., Scott, T., Dodet, G., Suanez, S., Jackson, D., Floc’H, F., 2016.
679 Extreme wave activity during 2013/2014 winter and morphological impacts along the
680 Atlantic coast of Europe. *Geophys. Res. Lett.* 43, 2135–2143.
681 <https://doi.org/10.1002/2015GL067492>

682 Masselink, G., Scott, T., Poate, T., Russell, P., Davidson, M., Conley, D., 2015. The extreme
683 2013/2014 winter storms: hydrodynamic forcing and coastal response along the
684 southwest coast of England. *Earth Surf. Process. Landforms* 41, 378–391.
685 <https://doi.org/10.1002/esp.3836>

686 May, V.J., Hansom, J.D., 2003. Hallsands, Coastal Geomorphology of Great Britain,
687 Geological Conservation Review Series.

688 McCarroll, R.J., Masselink, G., Valiente, N.G., Wiggins, M., Scott, T., Conley, D.C., King,
689 E. V., 2020. Impact of a headland-associated sandbank on shoreline dynamics.

690 Geomorphology 355, 107065. <https://doi.org/10.1016/J.GEOMORPH.2020.107065>

691 McCarroll, R.J., Masselink, G., Wiggins, M., Scott, T., Billson, O., Conley, D.C., Valiente,
692 N.G., Sciences, M., Circus, D., Hill, B., 2019. High-efficiency gravel longshore
693 sediment transport and headland bypassing over an extreme wave event 1–19.
694 <https://doi.org/10.1002/esp.4692>

695 Nicholls, R.J., Marinova, N., Lowe, J.A., Brown, S., Vellinga, P., de Gusmao, D., Hinkel, J.,
696 Tol, R.S.J., 2011. Sea-level rise and its possible impacts given a “beyond4°C world” in
697 the twenty-first century. *Philos. Trans. R. Soc. A Math. Phys. Eng. Sci.* 369, 161–181.
698 <https://doi.org/10.1098/rsta.2010.0291>

699 Plomaritis, T.A., Benavente, J., Laiz, I., Del Río, L., 2015. Variability in storm climate along
700 the Gulf of Cadiz: the role of large scale atmospheric forcing and implications to coastal
701 hazards. *Clim. Dyn.* 45, 2499–2514. <https://doi.org/10.1007/s00382-015-2486-4>

702 Ranasinghe, R., McLoughlin, R., Short, A.D., Symonds, G., 2004. The Southern Oscillation
703 Index, wave climate, and beach rotation. *Mar. Geol.* 204, 273–287.
704 [https://doi.org/10.1016/S0025-3227\(04\)00002-7](https://doi.org/10.1016/S0025-3227(04)00002-7)

705 Robinson, A.H.W., 1961. The Hydrography of Start Bay and Its Relationship to Beach
706 Changes at Hallsands. *Geogr. J.* 127, 63–77. <https://doi.org/10.2307/1793197>

707 Ruiz de Alegria-Arzaburu, A., Masselink, G., 2010. Storm response and beach rotation on a
708 gravel beach, Slapton Sands, U.K. *Mar. Geol.* 278, 77–99.
709 <https://doi.org/10.1016/j.margeo.2010.09.004>

710 Scaife, A.A., Yu Karpechko, A., Baldwin, M., Brookshaw, A., Butler, A., Eade, R., Gordon,
711 M., Maclachlan, C., Martin, N., Dunstone, N., Smith, D., 2015. Seasonal winter
712 forecasts and the stratosphere. *Atmos. Sci. Lett.* 17, 51–56.

713 <https://doi.org/10.1002/asl.598>

714 Scott, T., Masselink, G., Hare, T.O., Saulter, A., Poate, T., Russell, P., Davidson, M., Conley,
715 D., 2016. The extreme 2013 / 2014 winter storms : Beach recovery along the southwest
716 coast of England. *Mar. Geol.* 382, 224–241.
717 <https://doi.org/10.1016/j.margeo.2016.10.011>

718 Scott, T., Masselink, G., McCarroll, R.J., Castelle, B., Dodet, G., Saulter, A., Scaife, A.A.,
719 Dunstone, N., Atmospheric controls and long range predictability of directional waves in
720 the United Kingdom & Ireland., *Earth's Futur.* Submitted.

721 Splinter, K.D., Davidson, M.A., Golshani, A., Tomlinson, R., 2012. Climate controls on
722 longshore sediment transport. *Cont. Shelf Res.* 48, 146–156.
723 <https://doi.org/10.1016/j.csr.2012.07.018>

724 Stranack, D., 2017. The Lost Village of Undercliff, Blackawton and Strete History Group.

725 Thomas, T., Phillips, M.R., Williams, a T., 2013. A Centurial Record of Beach Rotation. *J.*
726 *Coast. Res.* 594–599. <https://doi.org/10.2112/SI65-101.1>

727 Trouet, V., Esper, J., Baker, A., Scourse, J., 2009. Persistent Positive North Atlantic
728 Oscillation Mode Dominated the Medieval Climate Anomaly Persistent Positive North
729 Atlantic Oscillation Mode Dominated the Medieval Climate Anomaly.
730 <https://doi.org/10.1126/science.1166349>

731 Trouet, V., Scourse, J.D., Raible, C.C., 2012. North Atlantic storminess and Atlantic
732 Meridional Overturning Circulation during the last Millennium: Reconciling
733 contradictory proxy records of NAO variability. *Glob. Planet. Change* 84–85, 48–55.
734 <https://doi.org/10.1016/j.gloplacha.2011.10.003>

735 UKHO, U.K.H.O., 2013. INSPIRE Portal & Bathymetry DAC [WWW Document]. Available

736 at. <http://aws2.caris.com/ukho/mapViewer/map.action>.

737 USACE, 2002. Shore Protection Manual. Government Printing Office, Washington, D.C.

738 van Rijn, L.C., 2014. A simple general expression for longshore transport of sand, gravel and
739 shingle. *Coast. Eng.* 90, 23–39.
740 <https://doi.org/https://doi.org/10.1016/j.coastaleng.2014.04.008>

741 Vos, K., Harley, M.D., Splinter, K.D., Simmons, J.A., Turner, I.L., 2019. Sub-annual to
742 multi-decadal shoreline variability from publicly available satellite imagery. *Coast. Eng.*
743 150, 160–174. <https://doi.org/10.1016/j.coastaleng.2019.04.004>

744 Wang, L., Ting, M., Kushner, P.J., 2017. A robust empirical seasonal prediction of winter
745 NAO and surface climate. *Sci. Rep.* 7, 279. <https://doi.org/10.1038/s41598-017-00353-y>

746 Waterhouse, R., 2009. Blackawton & Strete heritage appraisal: an archaeological history.
747 South Hams District Council, Totnes.

748 Weisheimer, Antje, Schaller, N., Reilly, C.O., Macleod, A., Palmer, T., Centre, E., Weather,
749 M., Ecmwf, F., Weisheimer, A, 2017. Atmospheric seasonal forecasts of the twentieth
750 century : multi-decadal variability in predictive skill of the winter North Atlantic
751 Oscillation (NAO) and their potential value for extreme event attribution. *Q. J. R.*
752 *Meteorol. Soc.* 143, 917–926. <https://doi.org/10.1002/qj.2976>

753 Wiggins, M., Scott, T., Masselink, G., Russell, P., Castelle, B., Dodet, G., 2017. The role of
754 multi-decadal climate variability in controlling coastal dynamics: re-interpretation of the
755 “Lost Village of Hallsands,” in: *Proceedings Coastal Dynamics 2017*. pp. 96–107.

756 Wiggins, M., Scott, T., Masselink, G., Russell, P., McCarroll, R.J., 2019a. Coastal
757 embayment rotation : Response to extreme events and climate control , using full
758 embayment surveys. *Geomorphology* 327, 385–403.

759 <https://doi.org/10.1016/j.geomorph.2018.11.014>

760 Wiggins, M., Scott, T., Masselink, G., Russell, P., Valiente, N.G., 2019b. Regionally-
761 Coherent Embayment Rotation : Behavioural Response to Bi-Directional Waves and
762 Atmospheric Forcing. *J. Mar. Sci. Eng.* 7, 116.

763 Worth, R.H., 1904. Hallsands and Start Bay. *Devonsh. Assoc.* 36, 302–346.

764